RI-225

V. G. Khlopin Radium Institute

I. D. Alkhazov, A. V. Kuznetsov,
V. I. Shpakov

FORMATION OF FRAGMENT MASS DISTRIBUTIONS IN SPONTANEOUS FISSION OF ^{252}Cf

PREPRINT

Moscow - Atominform - 1991

UDC 539.137.7 (047)

Alkhazov I. D., Kuznetsov A. V., Shpakov V. I. Formation of fragment mass distributions in spontaneous fission of ^{252}Cf: Preprint RI-225. - M.: Atominform, 1991. - 47 p.

The results of multiparameter measurements in binary and ternary spontaneous fission of ^{252}Cf are described. In the measurements the fragment kinetic energies and the numbers of neutrons emitted by each complementary fragment were registered. The fragment masses and kinetic energies were obtained for fixed specific combinations of the numbers of neutrons emitted by each fragment. The behaviour of the mass distributions as a function of fragment deformations is discussed. The character of mass distributions in binary and ternary fission is compared.

Алхазов И. Д., Кузнецов А. В., Шпаков В. И. Формирование массовых распределений спонтанного деления ^{252}Cf : Препринт РИ-225. - М.: ЦНИИатоминформ, 1991. - 47 с.

Описываются результаты многопараметровых измерений при при двойном и тройном спонтанном делении ^{252}Cf. В каждом акте деления регистрировались кинетические энергии обоих осколков и числа нейтронов, испущенных каждым из них. Получены распределения кинетических энергий и масс осколков для фиксированных комбинаций чисел испущенных нейтронов. Обсуждается поведение массовых распределений в зависимости от деформаций осколков. Сравнивается характер массовых распределений при двойном и тройном делении.

INTRODUCTION

One of the most important and still not cleared up problems of the nuclear fission mechanism is formation of fragment mass distributions. At present there exist a number of theoretical models based on different approaches which tend to describe with different degrees of confidence the fragment mass distributions and which, however, do not provide an exact quantitative solution of the problem. In particular, the statistical model [1], the fragmentation model [2], the scission point model [3], the model combining fission channels with the random neck-rupture [4, 5] can be mentioned among them. These models, although developed from different starting points, yield results which are mainly governed by the potential energy at the scission point and it can be shown that they are nearly equivalent from the qualitative point of view. This work is an attempt to get direct experimental information on the character of the potential energy surface in the scission point as well as on some details of the mass distribution formation.

EXPERIMENT

Multiparameter measurements of the fission process characteristics were performed in both binary and ternary spontaneous fission of ^{252}Cf. The following parameters were registered for each individual fission event: the kinetic energies of both complementary fragments, the numbers of neutrons emitted by each complementary fragment and the kinetic energy of long range particles in the case of ternary fission with equatorial and polar emission.

Neutrons were registered by a combination of two gadolinium loaded large liquid scintillation counters separated one from the other by a combined shield to prevent their mutual influence. The total neutron registration efficiency (including the geometry factors) amounted to 53%. Fission fragments were registered by a twin parallel plate ionization chamber with a collimation of the fragments within a small angle along the chamber axis.

The chamber was inserted into the center of the shield between the neutron counters. Long range particles were registered by silicon surface-barrier detectors arranged around the chamber electrodes inside the chamber.

In the measurements, 10^6 events of binary fission, 4.10^5 events of ternary fission with equatorial emission and 4.10^3 events of ternary fission with polar emission were utilized for experimental data processing.

The quality of the detector channels used can be characterized by the fragment pulse-height spectra (Fig. 1).

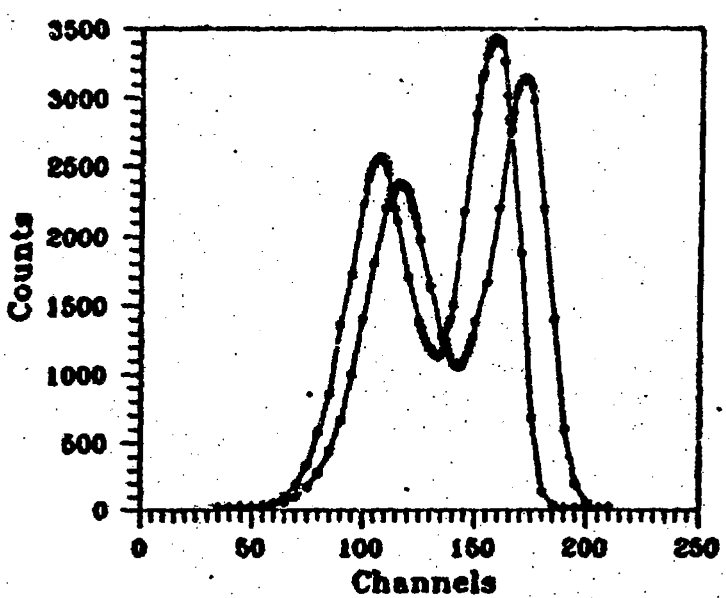

Fig. 1. The fission fragment pulse-height spectra

the preneutron fragment mass distribution in binary and ternary fission (Fig. 2), the long range particle pulse-height spectra for equatorial and polar emission (Fig. 3) and the saw-tooth dependence of the mean neutron emission on the fragment mass presented in Fig. 4 together with similar curves obtained by SIGNARBIEUX [6] and FRAENKEL [7].

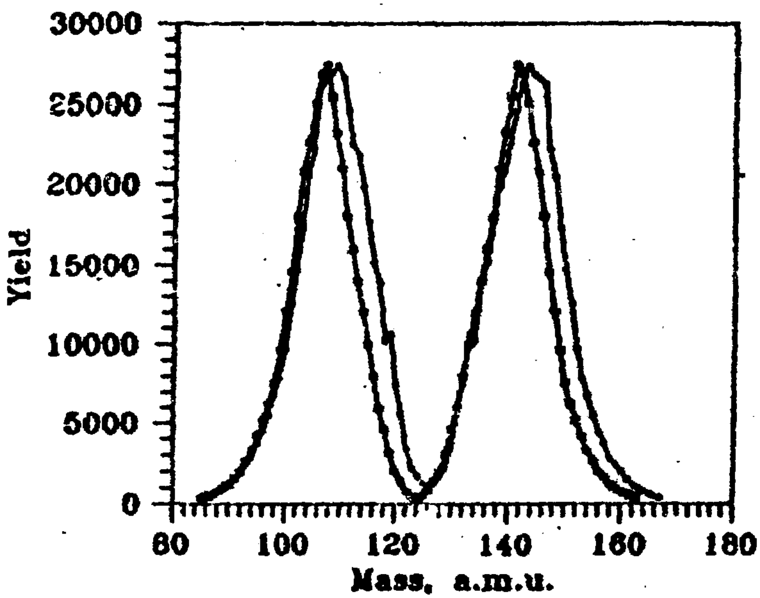

Fig. 2. Pre-neutron emission fragment mass distributions in binary and ternary fission

The measured two-dimensional multiplicity distributions $P(\nu_L,\nu_H)$ of neutrons emitted by both the light and the heavy fragments ν_L and ν_H were obtained in the measurements for each fixed fragment mass M and total kinetic energy E_K as raw experimental data. These distributions were then unfolded to obtain the initial distributions with corrections introduced

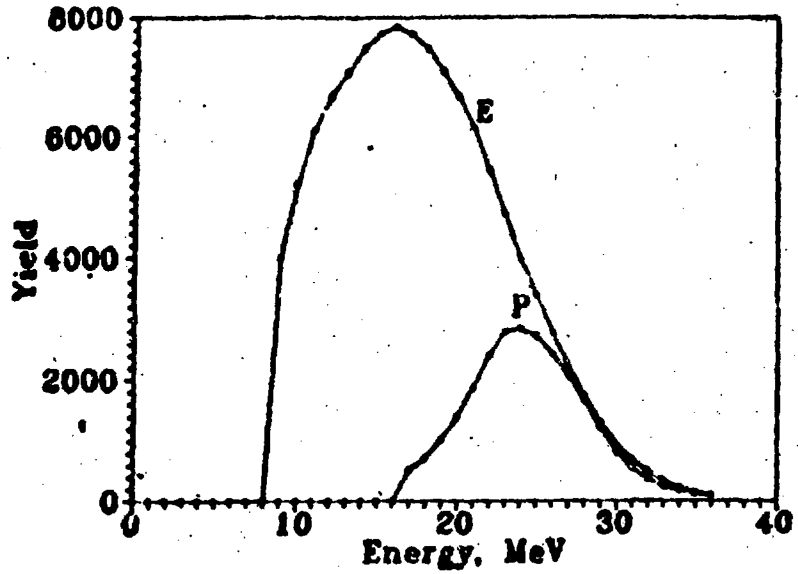

Fig. 3. The LR-particle energy spectra in ternary fission with equatorial and polar emission

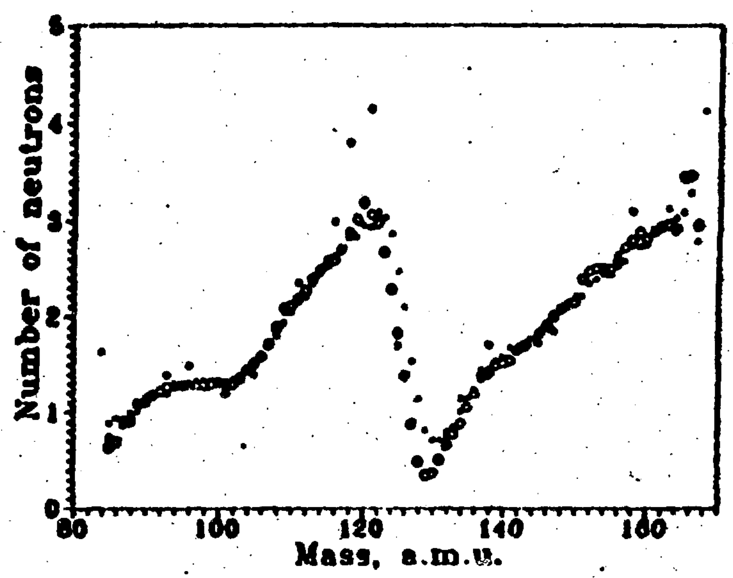

Fig. 4. The average neutron emission from individual fragments $\bar{\nu}$ as a function of fragment mass in binary fission: ▲- this work; o - data from ref. [6]; ● - data from ref. [7].

for the neutron detection efficiency, the background, and the neutron pulse pile-up. The finite mass and energy resolution at the fragment registration was also allowed for. A method of statistical regularization was employed to perform the $P(\nu_L,\nu_H)$ distribution unfolding by the use of prior information on both the smoothness and the momenta of the initial distributions. The initial $P(\nu_L,\nu_H)$ distributions thus obtained for various fixed M or E_K were then converted into distributions of preneutron masses $Y_M(\nu_L,\nu_H)$ and kinetic energies $Y_E(\nu_L,\nu_H)$ for fixed pairs of numbers of neutrons (ν_L,ν_H) emitted by the light and heavy fragments.The corrections for neutron emission introduced into M and E_K to obtain the preneutron values could be determined accurately enough since the numbers of neutrons were measured directly for each fission event.

The number of neutrons emitted is a direct measure of the fragment excitation energy, i.e. the sum of the energy dissipated at the descent from saddle to scission and the energy of deformation in the scission point.

On the basis of the existing estimation of free energy values (for example [8]), which does not exceed 10 MeV, it is possible to suggest that the dissipated energy can cause an emission of no more than one neutron. Therefore, the number of neutrons emitted is a measure reliable enough of fragment deformation in the scission point.

Consideration of mass distributions for fixed numbers of neutrons and thereby for fixed fragment deformation makes it possible to obtain information on the character of the potential energy surface in the scission point as well as on some quantum effects at the descent from saddle to scission. Such information can be compared with the nature of the potential surface obtained by WILKINS in the scope of the scission point model [3] and presented in Fig.5.

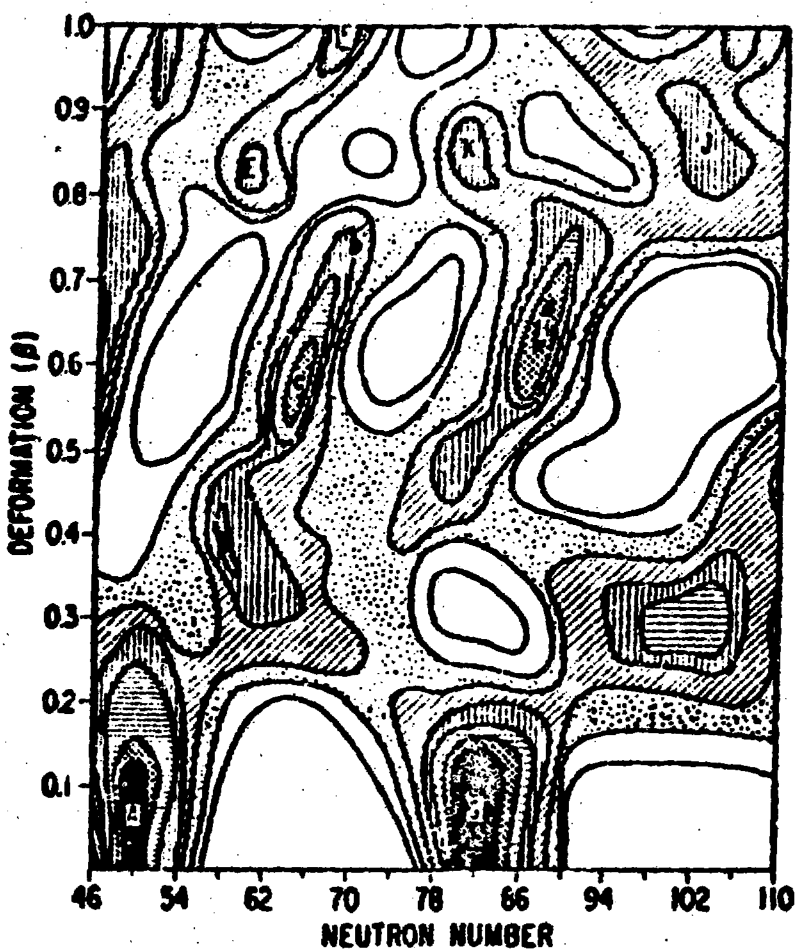

Fig. 5. Neutron- shell corrections calculated by Wilkins et al. [3] as a function of deformation (β) and neutron number.

. 'NARY FISSION

The fragment mass distributionsconsidered below are characterized by pairs of numbers $(\nu_L|\nu_H)$ which are the numbers of neutrons emitted by the light and heavy fragments.*)

The mass distribution corresponding to the case when no neutrons are emitted (0|0) and thus to the most compact configuration of both the fragments is presented in Fig. 6. It is characterized by two rather narrow main peaks at masses M_L=107, M_H=145 and by two pairs of satellite peaks at masses M_L=112, M_H=140 and M_L=102, M_H=150. A practically suppressed yield of mass M_H=132 can be noted, which corresponds to the double magic shell Z=50, N=82, and there by to the most deep minimum G in the potential energy plot at zero deformation of the heavy fragment, whereas masses M_H=140, 145, 150, are positioned at the slope of this minimum which corresponds to a greater potential energy.

It should be noted that the distribution considered is close to that obtained by BARREAU et al. [9] for true cold fission of ^{252}Cf (i.e. when Q-TKE < 6 MeV) and is presented in Fig. 7. Similar structures with a period of 5 a.m.u. can be seen in both distributions. Such structures that were found in a number of other studies (cf. [10, 11, 12]) can be regarded as

---

*) In our previous publication [24] similar symbols were used. However, there they denoted the numbers of neutrons emitted by the considered fragment (light in the left part of the Figures and heavy in the right part), and by the complementary one. In this paper these symbols denote the numbers of neutrons emitted by the light and the heavy fragments. Thus, in the previous paper publication the curves represented the left and the right parts of two different mass distributions, while now they are both halves of one mass distribution.

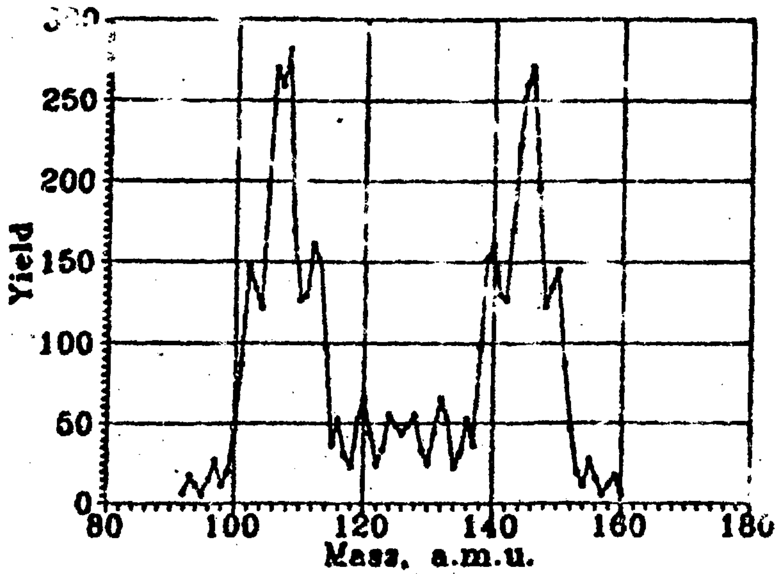

Fig. 6. The fragment mass distribution in binary fission

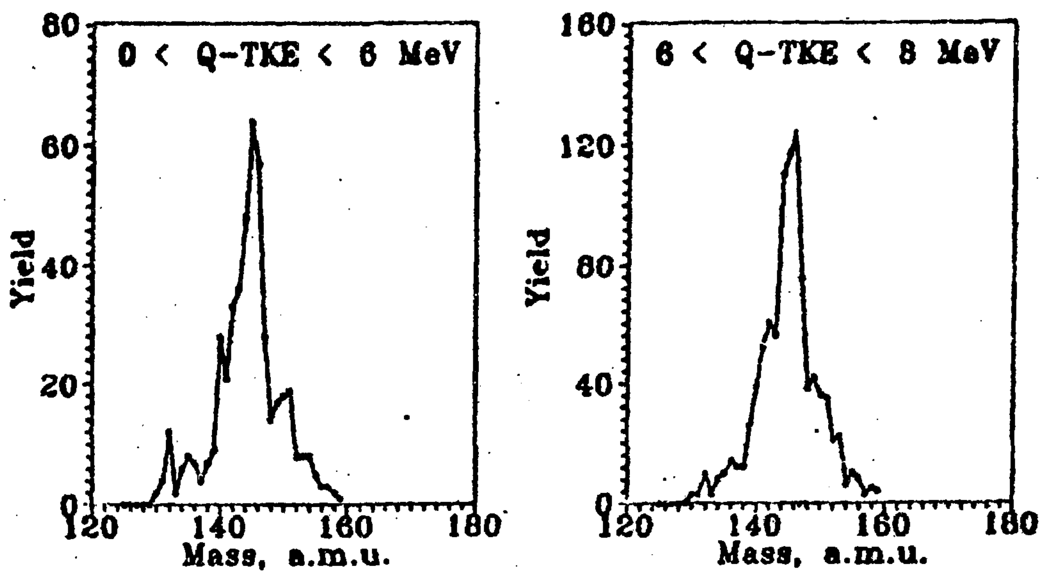

Fig. 7. The fragment mass distributions in cold compact fission of ^{252}Cf obtained in [9]

a well established and caused by the fragment charge even-odd effects. The presence of such structures caused by predominant mass yield of fragments with even charges is an evidence that the fission fragments are cold in the scission point because the proton pairing gap is less than 3 MeV.

The similarity of the distribution obtained in this work to that obtained by BARREAU et al. [9] and the presence of the structures mentioned shows that fission without neutron emission is cold enough in the scission point, though in this case Q-TKE = 10 MeV (cf. Table 4) and the fragment heating is not forbidden by the energy balance. It can be mentioned that in [9] the structures are also present in the energy interval of 6 MeV < Q-TKE < 8 MeV (cf. Fig. 7).

The mass M_H=132 appears when the light complementary fragment M_L=120 becomes deformed and its yield rises with the complement deformation increase as can be seen in Fig. 8 where the mass distributions for cases of (1|0), (2|0), (3|0), (4|0), (5|0) are presented. This can also be clear from distributions $P(\nu_L)$ and $P(\nu_H)$ for this fragment mass pair presented in Fig.9. The general trend of the behaviour of this fragment pair with the neutron numbers $(\nu_L|\nu_H)$ is presented in Table 1.

A compact fragment with the mass M=132 can thus exist only together with a deformed complement. This fact can be understood on the basis of a conclusion proposed by WILKINS [3] that the broad minimum on the potential energy surface at the quadrupole deformations $\beta_L=\beta_H$=0.6 due to a liquid-drop component causes the complement, the spherical fragment with N=82, to be very deformed. However, for the 107/145 mass split the liquid-drop component does not forbid both the fragments to be completely compact ($\nu_L=\nu_H$=0, Q-TKE < 10MeV). This difference can probably be associated with specific properties of light fragments M_L=107 and M_L=120, though they pertain to the same broad maximum in the contour plot (N_L=64 and N_L=72, respectively).

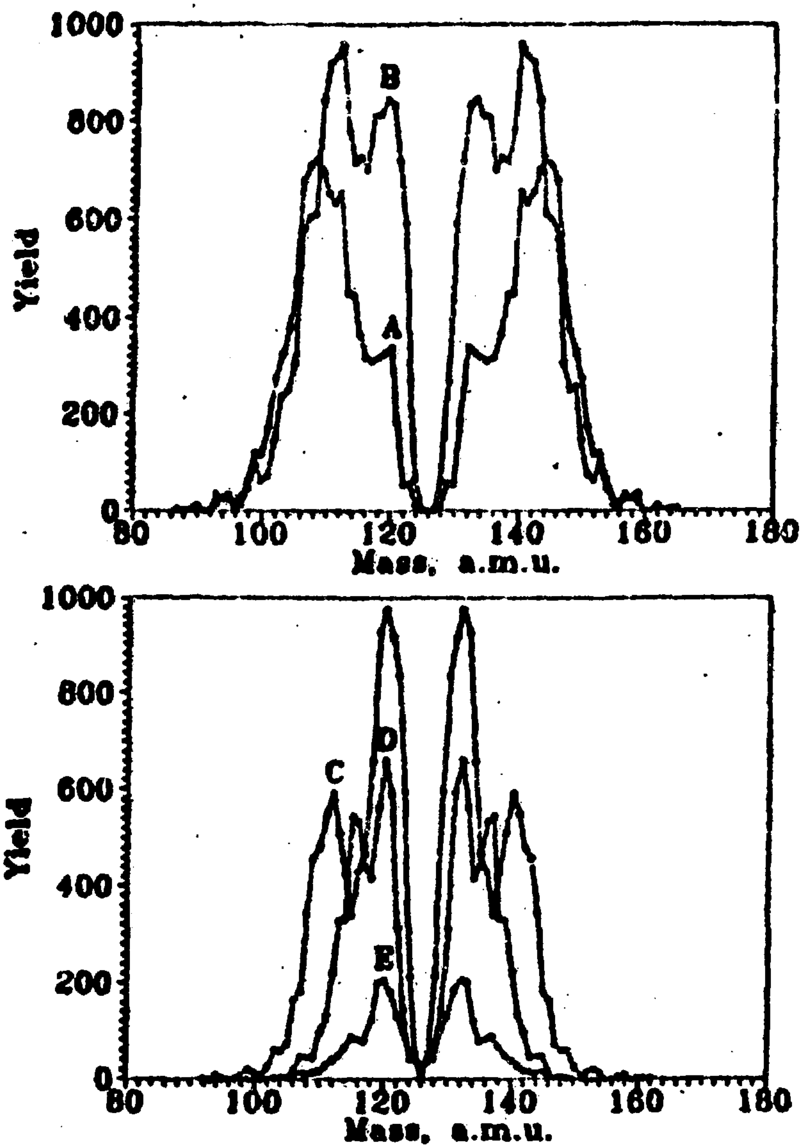

Fig. 8. The fragment mass distributions in binary fission for the fixed combination of neutron numbers:
A - (1|0); B - (2|0); C - (3|0); D - (4|0); E - (5|0)

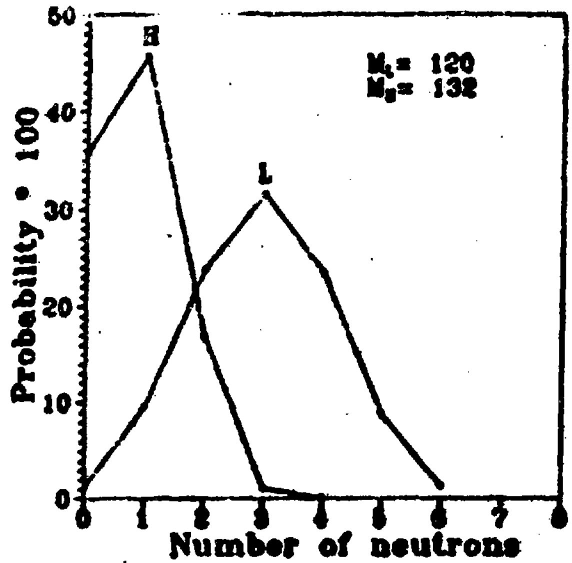

Fig. 9. The neutron multiplicity distributions $P(\nu_L)$ and $P(\nu_H)$ for the masses M_L=120, M_H=132 in binary fission

Table 1

Presence of the mass M_H=132 in the fragment mass distributions vs. the neutron numbers ν_L and ν_H emitted by the light and heavy fragments.

(Number 132 denotes combinations ($\nu_L|\nu_H$) in which an appreciable yield of this mass can be seen).

ν_L						
5	132	132	132			
4	132	132	132	132		
3	132	132	132			
2	132	132				
1	132					
0						
	0	1	2	3	4	5
						ν_H

It can be seen from Fig. 8 that the mass distributions for compact configurations of the heavy fragment consist of narrow pronounced peaks at masses M_H=145, 137-140, 132 and M_L= 107, 115- 112, 120 respectively. In this case the yield of mass M_H=145 drops quickly (disappears alredy in the case (2|0)) and the yield of masses M_H=137-140 or M_L=112-115 rises with the light fragment deformation increase. The last peak agrees well with the deformed minimum C, D in the contour plot by WILKINS and its mass increases from 112 to 115 in accordance with the slope of the C, D valley (N_L rises from 68 to 70). The general trend of the behaviour of mass M_L=112-115 with numbers of neutrons $(\nu_L|\nu_H)$ is presented in Table 2.

Table 2

Presence of mass M_L=112-115 in the fragment mass distributions vs. the neutron numbers ν_L and ν_H. (Figures denote both the presence of the mass and its variations with the neutron numbers increase).

ν_L						
5	115	114	114			
4	115	114	114	114		
3	112	114	114	112		
2	112	112	112			
1	112	112				
0	112					
	0	1	2	3	4	5

ν_H

There is no deformed minimum in the plot by WILKINS corresponding to the light mass M_L=120. Therefore, mass distributions for compact configuration of the heavy fragment can be assumed to be governed by quantum structures in heavy masses M_H=132, 145 and in light masses M_L=112-115.

When the deformation of the heavy fragment somewhat increases, the structures in the mass distribution and the character of their dependence on the light mass deformation remain generally the same. However, these masses can be found now at greater deformations of the light fragment, i.e. the mass M_H=145 disappears in the cases (2|2), (3|3), (3|4), and conversely the mass M_H=132 exists in the case (1|0), but disappears in the cases (2|1), (2|2), and at $\nu_H > 2$ (see Tables 1, 2 and 3).

The mass M_H=145 corresponds to the deformed minimum H in the plot by WILKINS (N_L=86-88) with the β=0.6 quadrupole deformation. However, the mass distributions obtained show that this mass exists and prevails in the case of the minimal deformation of both heavy and light fragments and still remains with the deformation increase (in general, this mass is the most pronounced in a broad range of the fragment deformations which is confirmed by the mean total mass of the heavy fragment peak $\bar{M}$ = 144.8 a. m. u.). In the case of the strongly deformed heavy fragment, themass M = 145 can be seen for a slightly more deformed light fragment (ν_L=1, 2, 3). When the light fragment is fully compact, this mass gradually shifts towards heavier values (M_H=147-150). The general trend in the behaviour of mass (M_H=145-150) against the numbers of neutrons ($\nu_L|\nu_H$) is presented in Table 3.

Mass distributions are rather narrow up to ν_H=3, but essentially broaden at ν_H=4, 5 due to a contribution of heavier masses, that is, to a more asymmetric mass split. In this case, these distributions can evidently be assumed to be governed by structures in the heavy mass, since they only slightly depend on the light fragment neutron numbers and for the cases (0|4),

Table 3

Presence of the mass M = 145-150 in the fragment mass distributions vs. the neutron numbers ν_L and ν_H. (Figures denote both the presence of the mass and its variations with the neutron number increase).

ν_L						
5						
4						
3				145	145	
2			145	145	145	145
1	145	145	145	148	150	
0	145	145	147	149	150	
	0	1	2	3	4	5

ν_H

(1|4), (2|4) or (0|5), (1|5), (2|5) are closely similar, as can be seen in Figs. 10 and 11, respectively.

Summing up the mentioned above, *one may assume the* existence of a well pronounced (N_H = 86 - 88) extended minimum, which is absent in the WILKINS plot, on the potencial surface at M_H = 144 - 146, beginning from small deformations up to the greatest ones, turning towars greater masses and essentially broadening with the growth of the heavy fragment deformation.

The general trend of the mass distribution behaviour with the fragment deformation increase can be noted. With the light fragment deformation increase, the mass peaks are shifted together toward the symmetric mass split. On the contrary, with the heavy fragment deformation increase, the peaks move apart toward the asymmetric mass split.

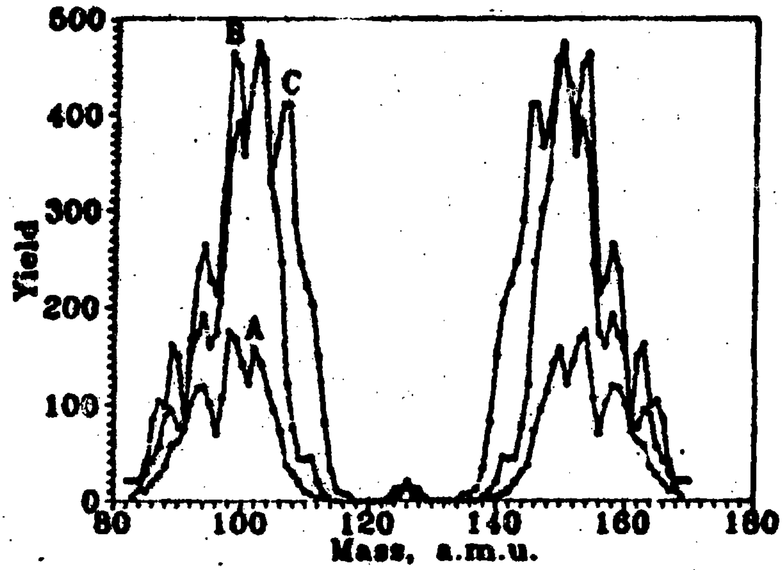

Fig. 10. The fragment mass distributions in binary fission for fixed combinations of neutron numbers: A - (0|4); B - (1|4); C - (2|4)

In the mass distributions shown in Figs. 8, 9, structures with a period of about 5 a.m.u. can be seen with peaks for similar masses M_L = 89, 94, 98, 102, 107, 112, and M_H = 163, 158, 154, 150, 145, 140. KNITTER et al. who measured the fragment charge directly [13] observed the same predominant masses in cold and nearly cold compact fission of ^{252}Cf, which were attributed to Z_L = 38, 40, 42, 44, even light fragment charges The presence of such structures can suggest that such strongly and asymmetrically deformed configurations can be cold in the scission point. The possibility of strongly deformed cold fission was theoretically predicted by HASSE [14] on the basis of the fact experimentally observed by NIFENECKER et al. [8] that the covariance of the numbers of neutrons emitted by coplementary fragments for fixed M is reduced to zero both at the maximal and minimal values of total kinetic energy.

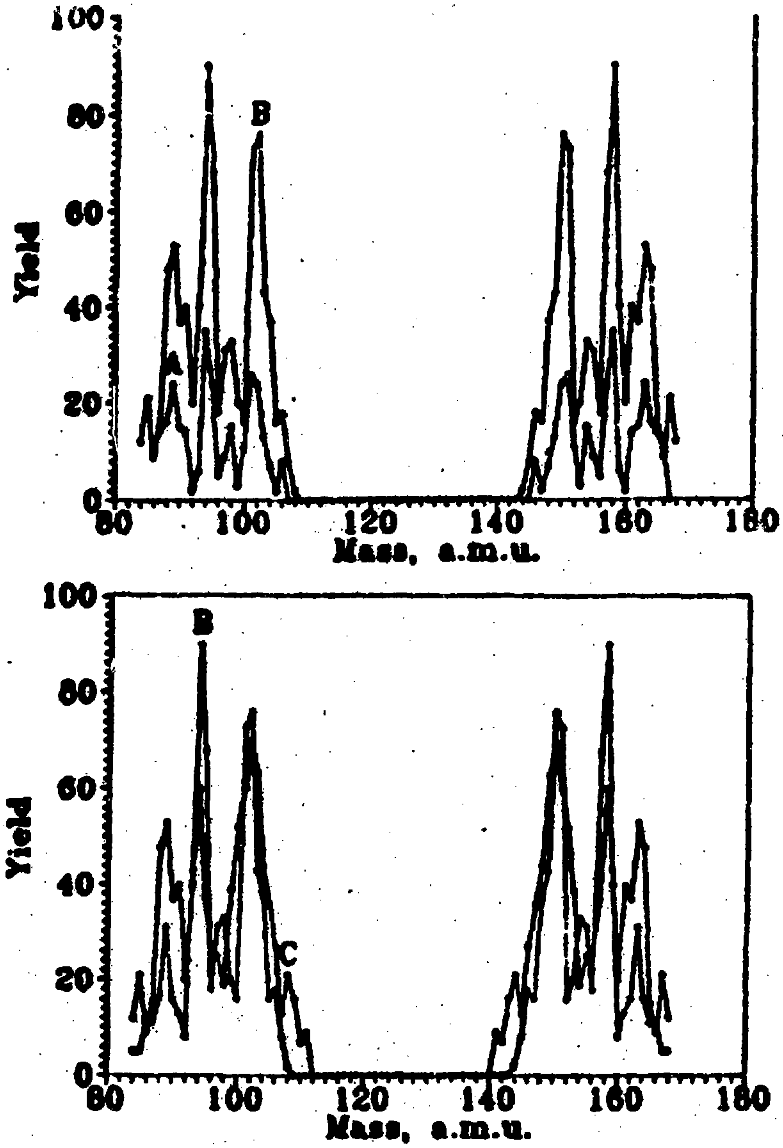

Fig. 11. The fragment mass distributions in binary fission for the fixed combinations of neutron numbers: A - (0|5); B - (1|5); C - (2|5)

A similar experimental fact was also obtained in this work (see Fig. 12). Following the calculations by NIFENECKER the zero value of $COV(\nu_L,\nu_H)$ corresponds to a zero variance of the fragment excitation energy which means reducing the free energy

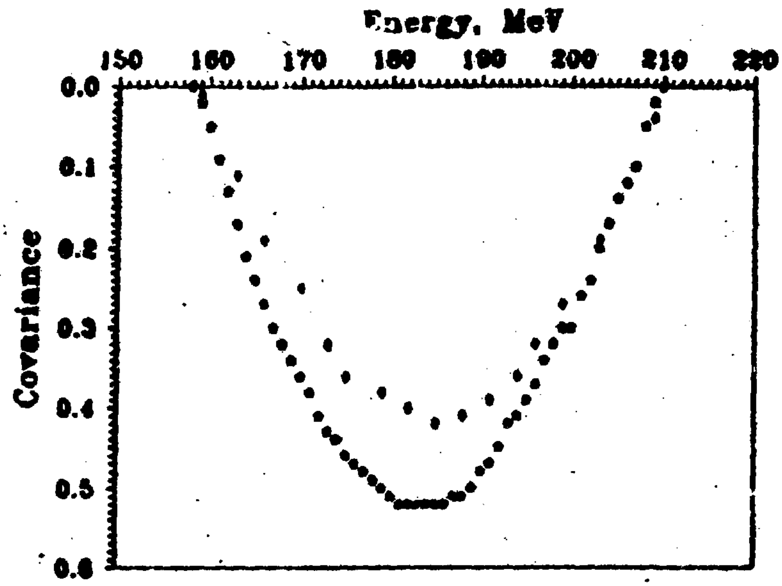

Fig. 12. cov(ν_L,ν_H) as a function of the fragment kinetic energy in binary fission:
- this work;
- curve from [6]

to zero, i.e. the difference between the energy available (Q) and the sum of potential energy components (Coulomb repulsion energy and the energy of fragment deformation) and thus the intrinsic excitation in the scission point. This situation can be illustrated by Fig. 13 in which the dependences of these potential energy components on the deformation are presented.

Cold deformed fission was experimentally observed in [15] in the thermal neutron induced fission of ^{245}Cm. The structures were found in the narrow energy ranges at both the maximal and minimal fragment total kinetic energies or at zero and maximal possible total excitation energies. The yield of such events is about of 10^{-4} - 10^{-5} of the total amount. The structures observed in this work are inherent in significantly wider

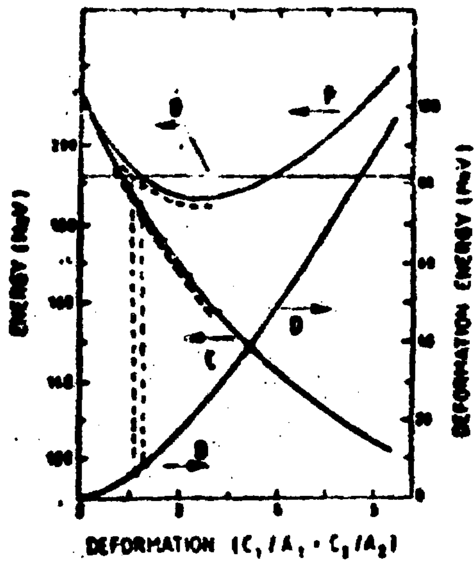

Fig. 13. Total deformation energy (D), Coulomb interaction energy (C) and potential energy (P) of the scission configurations limited by the total available energy (Q) from [14]

spread events and can be seen for case (0|4) i.e. at the total excitation close to its mean value (cf. $\bar{\nu}(^{252}Cf)$ = 3.76). In this case they can be assumed to be connected not only with the total excitation energy or with the total number of neutrons emitted, but rather with the asymmetry of their partition between the fragments as can be seen from Fig. 14, where the mass distributions are presented for various (ν_L, ν_H) cases at ν_T = 6. The range of total kinetic energy in which such structures are observed is much broader than that assumed from the starting point of zero free energy. It should be noted that similar structures were found by PIATKOV et al. [16] in the thermal fission of ^{233}U also in a broad range of TKE. It can be seen from Fig. 15 where the energy spectra from that paper are presented. The wide range of total kinetic energy makes one to assume that the cold deformed fission, if it really exists at

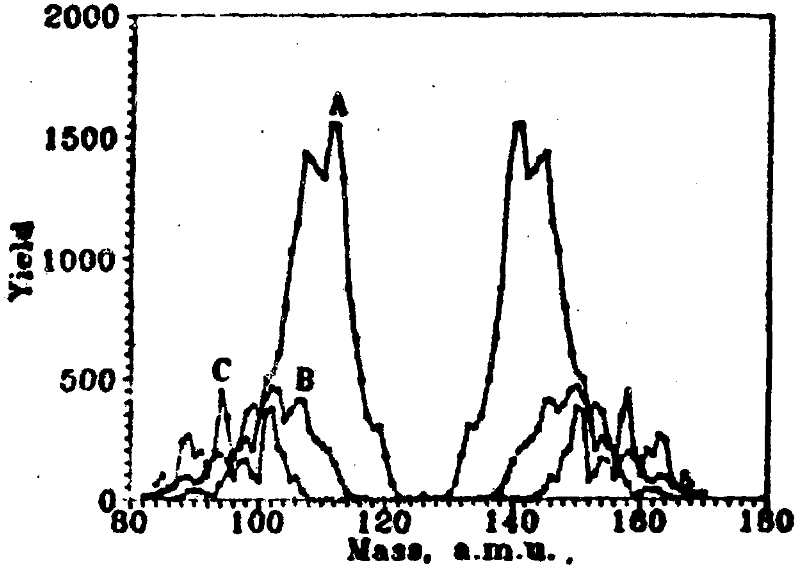

Fig. 14. The fragment mass distributions in binary fission for fixed combinations of neutron numbers:
A - (3|3); B - (2|4); C - (1|5)

all, occurs at non-zero free energy, and the free energy itself is not dissipated to the intrinsic excitation but is realized as a prescission kinetic energy and contributes to the fragment total kinetic energy, i.e. a superfluid descent from the saddle to scission can be assumed. It should be noted that in the range of deformations where the structures are observed, the total fragment kinetic energy is governed only by a deformation of the heavy fragment and does not depend on the light fragment deformation, i.e. remains the same for the cases (0|4), (1|4), (2|4), (3|4) or (0|5), (1|5), (2|5). (see Table 4). In this case the energy balance is not broken (cf. Table 6).

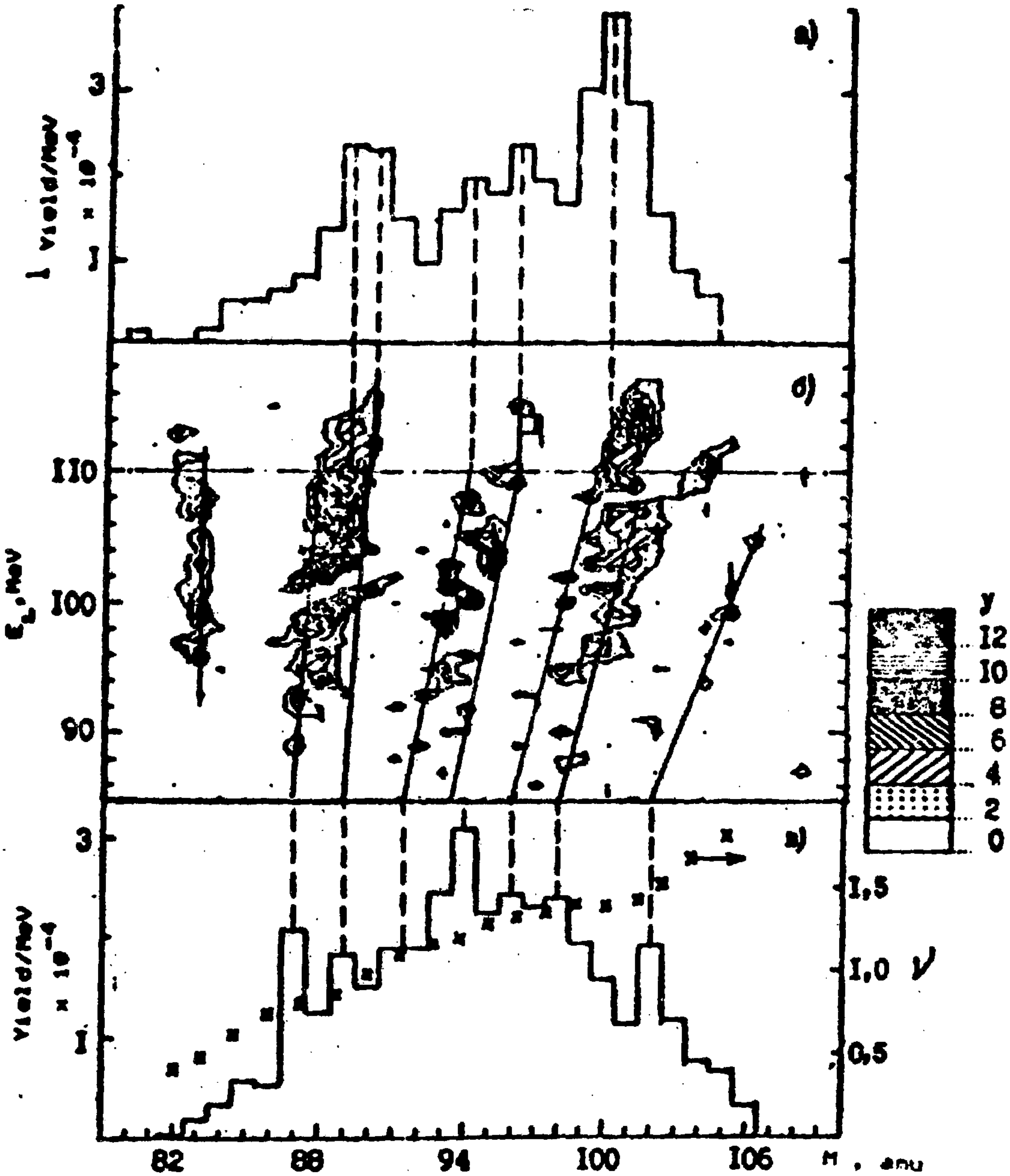

Fig. 15. Fine structures in the mass-energy distribution for the thermal neutron induced fission of ^{233}U from [16]:

a,c - the mass distributions at 110 MeV and 85 MeV total kinetic energies;

b - the mass-energy distribution;

x - the average neutron emission as a function of the light fragment mass

Table 4

Mean values of the fragment total kinetic energy (MeV) as a function of numbers of neutrons ν_L and ν_H.

ν_L							
6	170.5	173.0					
5	176.4	176.7	177.0				
4	182.8	182.1	181.0	178.0			
3	190.6	187.2	184.1	179.4	174.2		
2	197.1	191.7	186.4	181.0	174.6	168.4	
1	201.6	195.2	189.3	182.8	174.8	168.6	164.4
0	205.5	197.6	193.4	185.1	174.2	168.0	162.2
	0	1	2	3	4	5	6

ν_L

NIX and SWIATECKI [17] assumed that in the case of the superfluid descent the covariance of numbers of neutrons emitted by complementary fragments for fixed masses are expected to have an appreciable negative value .The dependence of COV(ν_L,ν_H) averaged over the total kinetic energy on the fragment mass obtained in that work is presented in Fig. 16. It can be seen that in the range of masses where thestructures exist a noticeable negative covariance can be observed.

If one assumes a superfluid descent in some region of fragment mass or deformations, then a dependence of the viscosity parameter on the fragment mass or deformation has to be assumed. Such a dependence could be understood, in particular, if a viscosity mechanism accounting for Landau-Zener transitions [18] was considered. In this case, the level bunching and due to it different probabilities of transitions on upper or lower levels could cause such a dependence of viscosity and other dynamic effects on the fragment mass split.

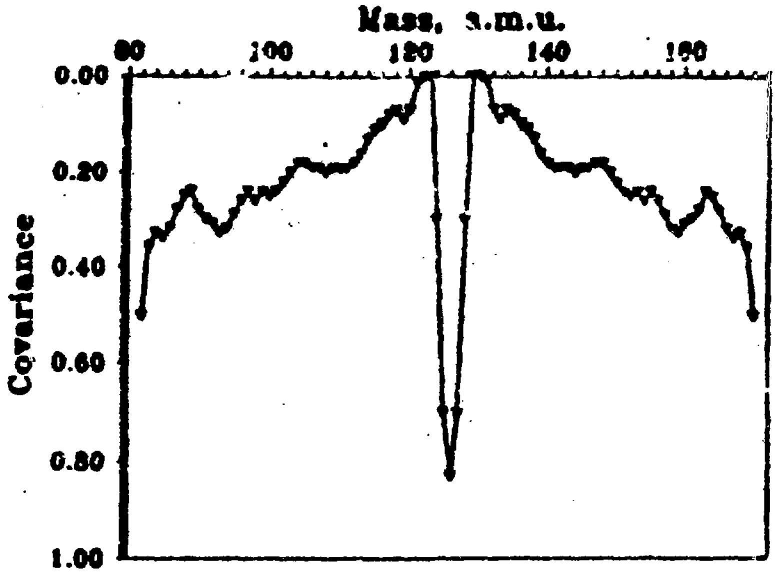

Fig. 16. COV(ν_L,ν_H) as a function of fragment mass

Mean values of the fragment total kinetic energies are presented in Table 4. A constancy of the TKE with heavy fragment deformation can be seen for large deformations of light fragments similar to that for a large deformation of heavy fragments (cf. cases (4|0), (4|1), (4|2) and (5|0), (5|1), (5|2)). It is possible that in this case fission can also be cold in the scission point, but the structures with a period of 5 a.m.u. can not be observable because the peaks are now too narrow.

Another fact can be noted in Table 4. In the case of strong deformations of heavy fragments, the TKE values are less than those for strong deformations of the light fragments. This fact is in good agreement with the energy balance, since in the first case the mass distribution is strongly asymmetric for which the Q- value is much less than in the second case where the mass split is close to a symmetric one and the Q-value is the highest possible. The lower TKE values in the first case suggest that heavy fragments are more deformable or softer though they are considered traditionally to be more stiff.

On the basis of measured neutron multiplicities the total excitation energy as a function of the fragment mass was calculated. The statistical model using the Hauser-Feschbach method was employed [19]. The results of the calculations together with the TKE values measured were in good agreement with the energy balance except for the symmetric region. The Q-values were taken from [20]. The results of the calculations and the comparisons are presented in Table 5. However, in the cases of large deformations of one of the fragments, Q - $\overline{TKE}$ value differs from the calculated excitation energy in a different way depending on what fragment is deformed. Some of these values are presented in Table 6. If the heavy fragment is strongly deformed, that is, when the structures in the mass

Table 5

Comparison of mean total excitation energies for various fragment masses calculated on the basis of measured numbers of neutrons [19] with differences $\overline{Q}$ - $\overline{TKE}$.

M_L a.m.u.	E^*_L MeV	E^*_H MeV	TKE MeV	Q [20] MeV	Q - TKE MeV	$E^*_L + E^*_H$ MeV
96	12.9±4.0	19.7±5.0	174±3	209	35	32.6
100	13.9	17.4	178	210	32	31.3
104	16.9	15.6	181	213	32	32.5
108	17.8	14.7	184	217	33	32.5
112	21.9	13.6	186	223	37	35.5
116	22.1	13.9	188	228	40	36.0
120	25.2	13.1	191	232	41	38.3
123	23.9	12.6	190	233	43	36.5
125	19.2	16.7	188	233	45	35.9

distributions are seen, the calculated excitation energies are systematically higher than the Q - TKE differences which suggest a deficit of energy spent for an intrinsic excitation.

A peculiar character of the neutron multiplicity distributions in symmetric and nearly symmetric regions should be noted. Starting from the mass M_L = 123, M_H = 129, the distributions become bimodal. In the distribution $P(\nu_L)$ for the mass M_H = 129 corresponding to the compact configuration, a

Table 6. Comparison of the mean total fragment excitation energies calculated on the basis of measured numbers of neutrons [19] for cases of a large asymmetry of the fragment deformations with the differences $\overline{Q - TKE}$.

$(\nu_L \| \nu_H)$	Q MeV	TKE MeV	Q - TKE MeV	E^* MeV
0|1	216	197.6	18.4	18.5
0|2	214	193.4	19.6	24.0
0|3	212	185.1	26.9	30.2
0|4	210	174.6	35.4	38.0
0|5	208	168.0	40.0	45.4
1|2	216	189.3	26.7	31.1
1|3	213	182.8	30.2	36.4
1|4	212	174.8	37.7	45.9
1|5	208	168.6	39.4	53.3
1|1	219	195.2	23.8	24.1
1|0	221	201.6	19.4	18.6
2|0	227	197.1	29.9	26.6
3|0	229	190.6	38.4	31.1
4|0	233	182.8	50.2	41.7
5|0	235	176.4	58.6	49.1
2|1	227	191.7	35.3	32.3
3|1	230	187.2	43.3	37.6
4|1	235	182.1	52.9	45.7
5|1	235	176.7	58.3	52.0

second mode characteristic for an elongated configuration arises. In the symmetric mass split both distributions for M_L = 126 and M_H = 126 are similar and have two pronounced modes with the same yields. The distributions are presented in Fig. 17. The two-dimensional distribution $P(\nu_L,\nu_H)$ for the

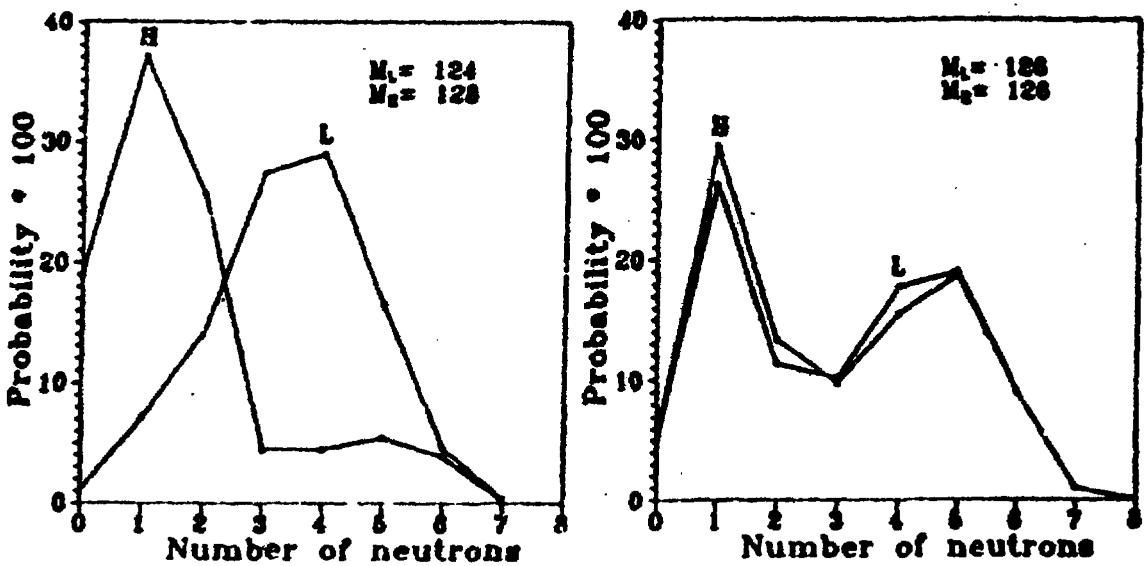

Fig. 17. The neutron multiplicity distributions $P(\nu_L)$ and $P(\nu_H)$ for the fragment mass pairs M_L= 124, M_H= 128 and M_L= M_H= 126

symmetric mass split is presented in Fig. 18. Two types of fission configurations can be seen in this distribution: for moderate and equal deformation of both fragments and a combination of a compact fragment with a strongly deformed complement. The second type can be due to Z = 50 proton shell. The presence of two types of scission configurations can also stem from two valleys in descent from the saddle to scission predicted by BROSA and GROSSMAN [4,5].

	0	1	2	3	4	5	6	7	8
0					13	23	17	3	
1		9		53	113	106	62		
2			22	33	31	48	16	5	1
3		44	25			24	5		
4	13	97	20		32	11	5	2	1
5	23	96	43	28	11	5	2		
6	17	60	16	5	5	2	1		
7	5		5						
8			1		1				

Fig. 18. The two-dimensional neutron multiplicity distribution $P(\nu_L, \nu_H)$ in binary fission for symmetric mass split

TERNARY FISSION WITH EQUATORIAL EMISSION OF LONG RANGE PARTICLES

Silicon surface-barrier detectors used for the long range particle registration failed to distinguish the type of particles. Therefore, all the information obtained was attributed to α-particles since their emission is the most probable. Besides, at the present stage of data processing the information on the LR-particle energy was omitted in the data interpretation because of a complexity of dealing with five-dimensional spectra and was used only for calculations of corrections for the LR-particle recoil.

The mean values of different quantities in ternary fission are presented in Table 7 in comparison with similar data from [21,22] and with similar quantities in binary fission. The saw-

Table 7

Mean values of various quantities in binary and ternary fission of ^{252}Cf.

Binary fission			
	[22]	[21]	This work
E_k, MeV	186.26±0.01	187.3±0.1	186.8±0.1
M_L, a.m.u.	108.5	108.7±0.1	108.6±0.1
M_H, a.m.u.	143.4	143.3±0.1	143.4±0.1
ν_T	3.766±0.002		
ν_L/ν_H	1.16	1.13	1.13
Ternary fission			
E_k, MeV	169.79±0.04	174.5±0.1	175.4±0.1
$E_k^{BF}-E_k^{TF}$, MeV	13.56±0.04	12.8±0.1	11.4±0.1
M_L, a.m.u.	106.2	105.9	106.6±0.1
M_H, a.m.u.	141.8	142.1	141.4±0.1
ν_T	3.072±0.006	3.11±0.05	3.06±0.01
ν_L/ν_H	1.13		1.12
Statistics	70000	8500	450000

tooth curves of the average neutron emission from individual fragments as a function of fragment mass in binary and ternary fission are presented in Fig. 19. It can be seen that both curves are rather similar in shape except for a shift towards lower ν values in the latter case. When the mass distribution in ternary fission is compared with that in binary fission, then a similar shift by 2 a.m.u can be seen both in the peak positions and in the mean values of the light and heavy

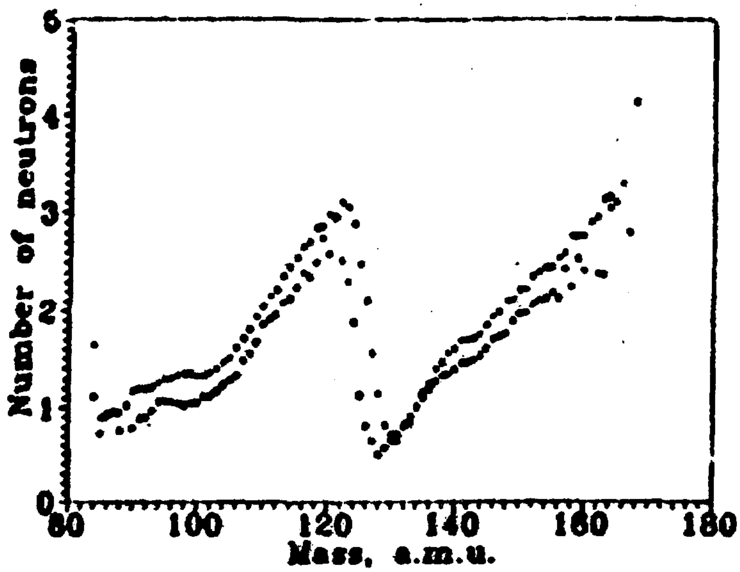

Fig. 19. The mean neutron emission as a function of fragment masses in binary and ternary fission with equatorial emission of LR - particles

fragments. This fact is in agreement with the results obtained by other authors (for example [20]).

General behaviour of the partial fragment mass distributions for fixed combinations (ν_L, ν_H) in ternary fission is the same as in binary fission, but nevertheless there are some appreciable distinctions, which probably stem from the LR-particle emission.

Mass distribution with no neutron emission (Fig. 20) represents narrow peaks just like those in binary fission, but with masses shifted by 2 a.m.u. (i.e. M_L=105, M_H=143). The mass deficit in this case is thus the same as for the total mass distribution and is equal in both the light and heavy fragments. Besides these peaks, satellite peaks can be seen with masses M_L=100 and M_H=148 corresponding to the masses

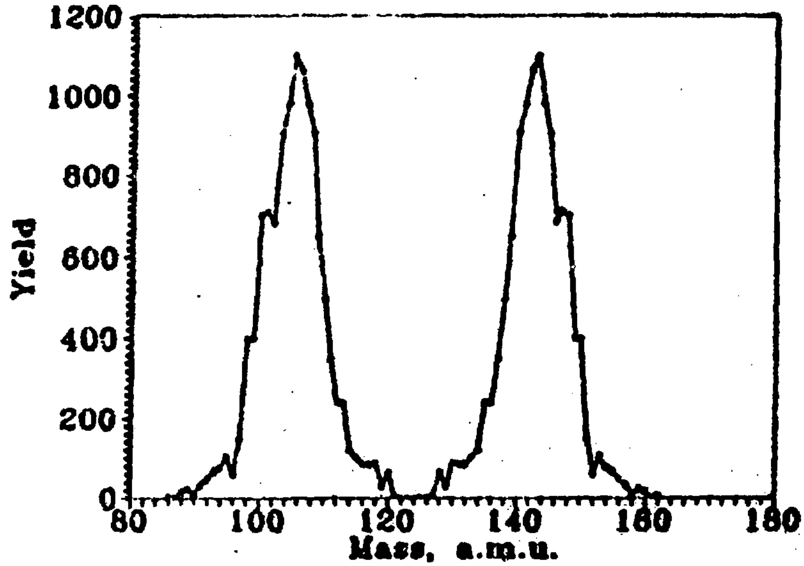

Fig. 20. The fragment mass distribution in ternary fission for the case (0|0) when no neutrons are emitted

M_L = 102 and M_H = 150 in binary fission. The double magic mass M_H = 132 is absent as in binary fission. Therefore, the cold ternary fission can be suggested to be similar to cold binary fission but the main mass M_H=145 now shifted due to the LR-particle emission.

Yield of the M_H=132 double magic mass rises with the light fragment deformation increase as was in binary fission. This situation can be seen in Fig. 21 where mass distributions for the cases of (1|0), (2|0), (3|0), (4|0), (5|0) are presented and also in Fig. 22 where neutron multiplicity distributions $P(\nu_L)$ and $P(\nu_H)$ for the M_L=105, M_H=143 and M_L=116, M_H=132 mass pairs are shown. A comparison of these distributions with those in binary fission shows them to have approximately the same character, but to be appreciably narrower or shorter. It can

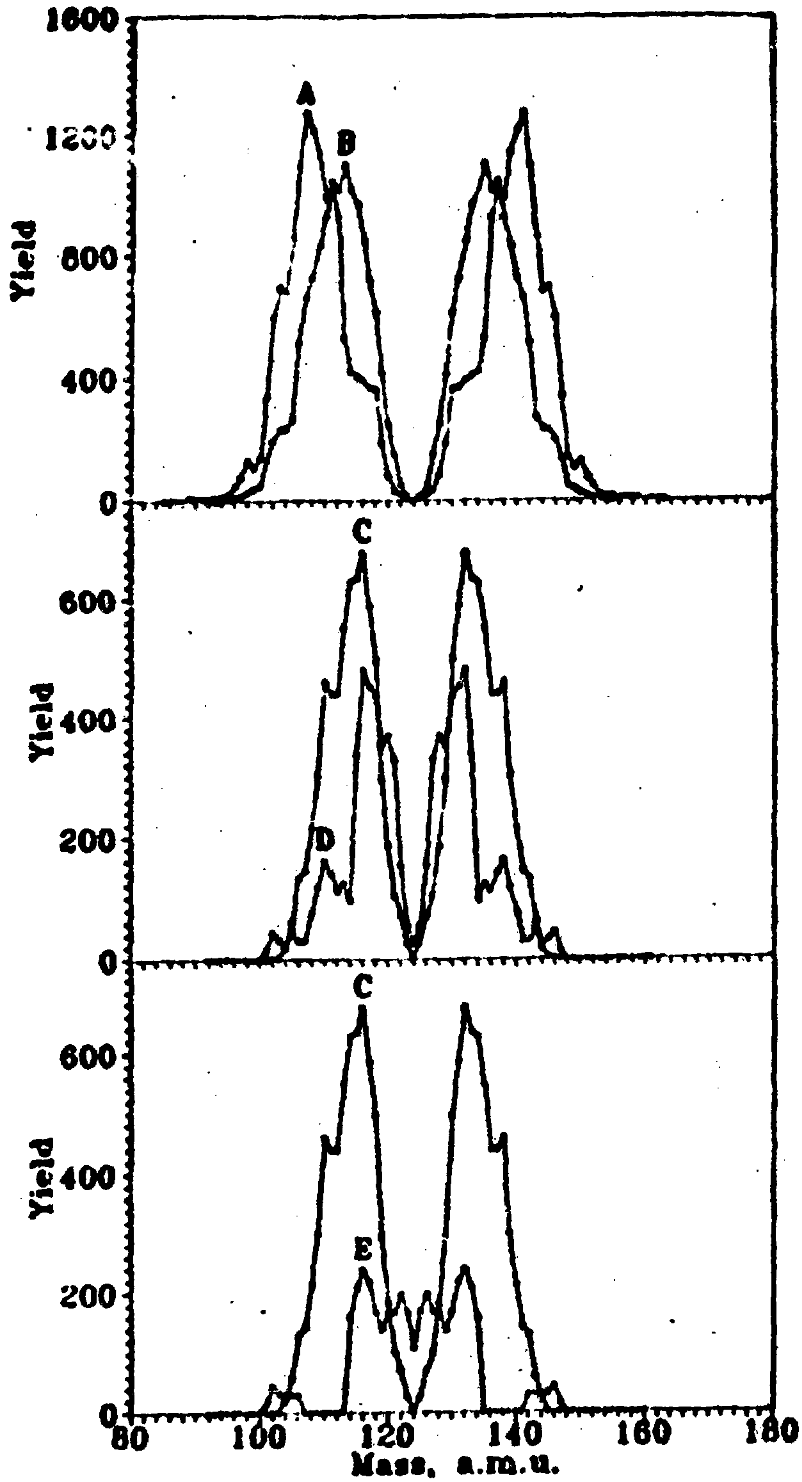

Fig. 21. The fragment mass distributions in ternary fission for fixed combinations of neutron numbers: A - (1|0); B - (2|0); C - (3|0); D - (4|0); E - (5|0)

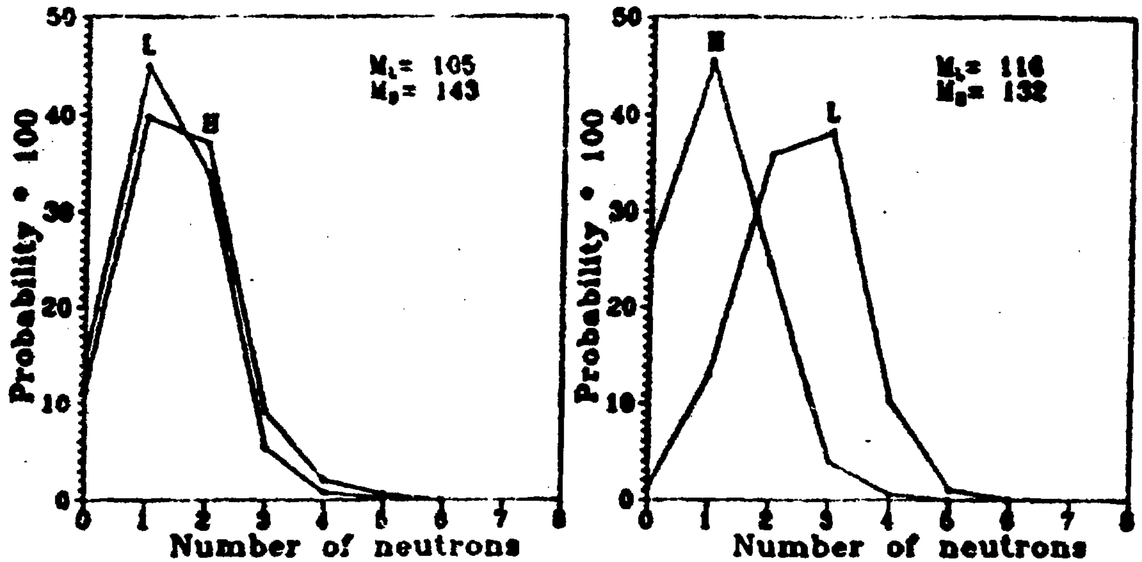

Fig. 22. The neutron multiplicity distributions $P(\nu_L)$ and $P(\nu_H)$ in ternary fission for the fragment mass pairs M_L = 105, M_H = 143 and M_L = 116, M_H = 132

be seen in Fig. 21 that the mass M_H=132 is well pronounced and is not shifted, which makes it possible to assume that the fragment corresponding to double magic shell does not contribute to the α-particle formation. Yield of the mass M_H=132 occurs for the same combinations of neutron numbers as in binary fission, i.e. (1|0) to (5|0), (3|1) to (5|1), (3|2)

Equal displacement of both the peaks in ternary fission by 2 a.m.u. with respect to those in binary fission can be seen only for a limited set of (ν_L,ν_H) cases, corresponding to small numbers of neutrons or small deformations. In the case of large and asymmetric deformations a shift of only one peak by 4 a.m.u. can be seen, corresponding to a fragment which is more deformed or emits many neutrons, with the mass of the complementary fragment being the same as in binary fission. The general trend of such a dependence of the fragment mass shifts on the fragment deformations or on the numbers of neutrons emitted is presented in Fig. 23 where L and H denote the shift of only one peak (light and heavy ones, respectively) and E_q denotes a simultaneous shift of both peaks by 2 a.m.u.

5	L	L	L			
4	L	L	L	L		
3	L	L	L	H	H	
2	Eq	L	Eq	Eq	H	H
1	Eq	Eq	Eq	Eq	H	H
0	Eq	Eq	Eq	H	H	H
	0	1	2	3	4	5

Fig. 23. The shifts of the mass distribution peaks in ternary fission with respect to those in binary fission as a function of neutron numbers ν_L and ν_H. L and H denote the shift of only one light or heavy peak, respectively. E_q denotes an equal shift of both the peaks

An example of such an equal shift of both peaks is shown in Fig. 24 where the mass distributions in binary fission (BF) and ternary fission (TF) are presented for the (2|2) case.

An example of the light fragment shift for the (4|0) case is shown in Fig. 25. In the distribution of binary fission, two pairs of peaks for masses M_L=115, 120 and M_H=137, 132 can be seen. In the distribution for ternary fission both peaks which belong to heavy masses remain the same, whereas the peaks of light masses are shifted by 4 a.m.u. and become M_L = 116, 110. It should be noted that due to heavy masses to be retained in ternary fission for strong deformations of light fragments the same components can be seen in the mass distributions in binary and ternary fission, i.e. M_H=132 and 137-138, whereas the

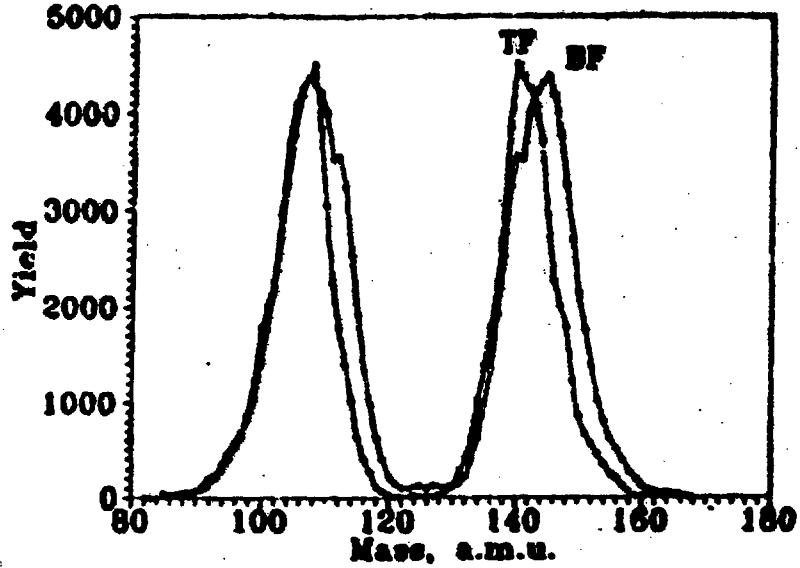

Fig. 24. The mass distributions in binary and ternary fission for the case of the (2|2) combination of fixed neutron numbers.

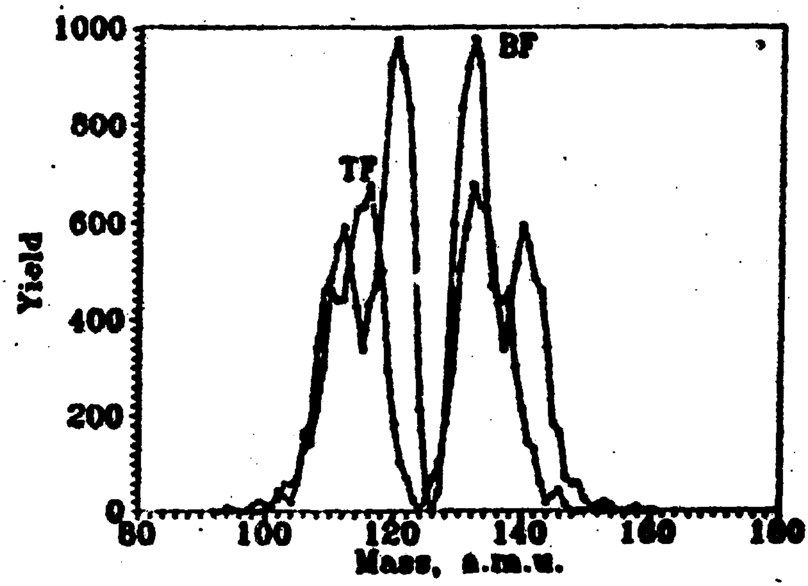

Fig. 25. The mass distributions in binary and ternary fission for the case of the (3|0) combination of fixed neutron numbers

complementary components of the light fragment masses in ternary fission are shifted by 4 a.m.u. with respect to those in binary fission and are now M_L=116 and M_H=110-111 instead of M_L=120 and M_L=114-115. Their behaviour vs. the light fragment deformation is the same as in binary fission, though in ternary fission the latter mass appears in slightly greater deformations of the light fragment. If in binary fission this mass can be seen in the case of ν_L=0, then in ternary fission it appears only with ν_L=1 or even ν_L=2. As mentioned above, this mass determines the formation of fragment mass distributions in the case of strong deformations of light fragments and is governed by the minimum C, D on the plot by WILKINS.

The behaviour of the mass corresponding to the mass M_L=145 in binary fission vs. fragment deformation in both cases is the same. However, in the case of ternary fission it is more difficult to identify this mass because it is shifted by 2 a.m.u. (M_H=143) for small fragment deformations and by 4 a.m.u. for large fragment deformations and increases at the same time with a rise in the heavy fragment deformation.

Broadening of mass distributions at ν_H=4, 5 occurring in binary fission can also be observed in ternary fission. However, now it can be seen for a smaller number of neutrons emitted by the heavy fragment i.e. at ν_H=3. All the facts mentioned make it possible to suggest that the valley on the energy surface at M_H=88-94 assumed for the binary fission governs mass distributions in ternary fission as well. An example of a shift in the heavy mass in ternary fission for a large deformation of the heavy fragment can be seen in Fig. 26 where mass distributions in binary and ternary fission are presented for the case (1|4). A series of peaks for the masses M_L = 89, 94, 98, 102, and M_H = 163, 158, 154, 150, can be seen in binary fission. In ternary fission, the same peaks exist in the light mass distribution (i.e. M_L = 90, 94, 98, 102), but the peaks corresponding to heavy masses are shifted by 4 a.m.u. (M_H = 158, 154, 150, 146).

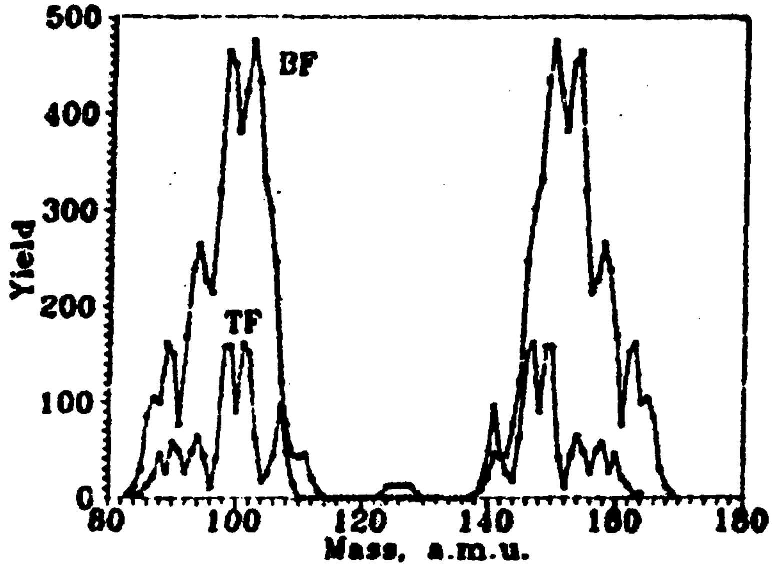

Fig. 26. The mass distributions in binary and ternary fission for the case of the (1|4) combination of fixed neutron numbers

All the facts mentioned show that formation of the mass distributions is governed by the same relief of the potential energy surface both in the binary and ternary fission and the scission configurations in both cases is nearly the same. The main contribution of nucleons to LR-alphas formation is in our opinion brought by one fragment, which agrees with the assumption by Peather [23]. Here the LR-particles are emitted most probably by a more deformed fragment. In the cases of small and equal deformations of both fragments each fragment can contribute 4 nucleons with the same probability which leads to an averaged mass distribution with a mean mass shift by 2 a.m.u. This situation is illustrated in Fig. 27 where mass distributions for the case (2|3) are presented. For binary fission, the peaks at M_L=107, M_H=145, are seen, whereas for

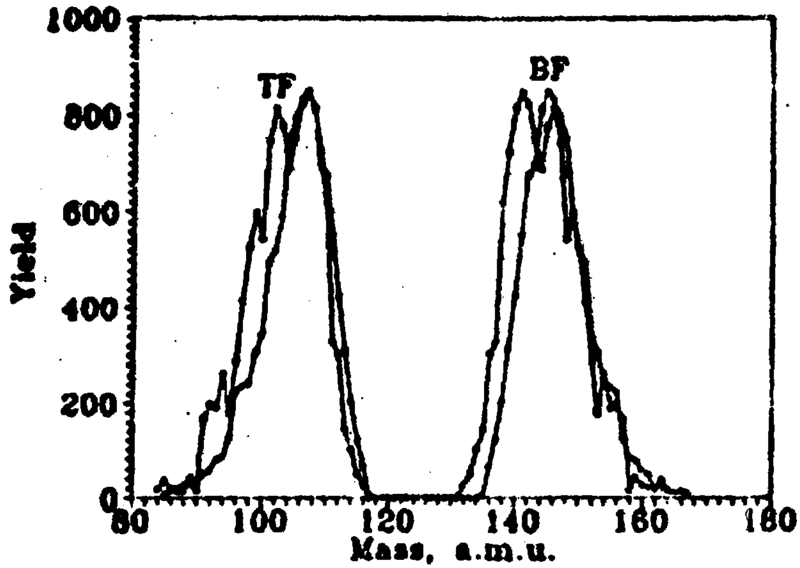

Fig. 27. The mass distributions in binary and ternary fission for the case of the (2|3) combination of fixed neutron numbers

ternary fission there are two pairs of peaks at M_L = 102, 107, and M_H = 146, 141, which either correspond to binary fission or are shifted by 4 a.m.u.

For large deformations of heavy fragments in ternary fission, i.e. at $\nu_H \geq 4$ (as can be seen in particular in Fig. 26) structures with a period of about 5 a.m.u. can be found in fragment mass distributions similar to those seen in binary fission. Thus, a conclusion can be made that cold deformed fission may also exist in ternary fission. It should be emphasized that the peaks of these structures are seen in all cases for the same light masses both in binary and ternary fission. This certainly stems from the fact that LR-alphas are mainly emitted by more deformed heavy fragments. These structures exist in the region of small statistics and therefore are not always statistically confident. Nevertheless, it should be pointed out that these structures were systematically repeated for the same masses in three independent measurements: in our former work [24] and in two sets of data independently processed for binary and ternary fission obtained in this work.

In ternary fission for large deformations of one of the fragments, the total fragment kinetic energy does not change with the deformation of the complementary fragment, i.e. remains the same for the cases (0|4), (1|4), (2|4), (3|4), or (0|5), (1|5), (2|5), as well as it is in binary fission.

In the region of symmetric fission, neutron multiplicity distributions in ternary fission have the same bimodal character as in binary fission. It can be seen in Fig. 28 where the $P(\nu_L)$ and $P(\nu_H)$ are presented for the symmetric mass split $M_L = M_H = 124$. Thus, in ternary as well as in binary fission there exist two versions of configuration with intermediate and equal deformations and a combination of compact fragments with strongly deformed ones.

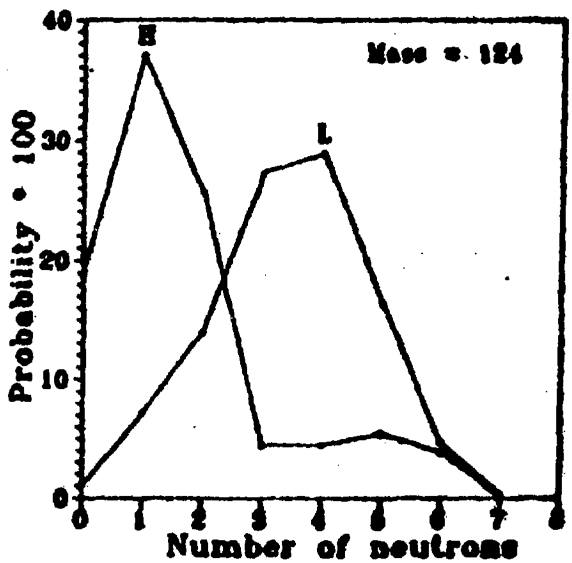

Fig. 28. The neutron multiplicity distributions $P(\nu_L)$ and $P(\nu_H)$ in ternary fission for the symmetric mass split ($M_L = M_H = 124$)

TERNARY FISSION WITH POLAR EMISSION OF LONG PARTICLES

It is evident now that the term "polar emission" can be used only conditionally because such emission occurs over the angles from 0 to 180° with respect to the fragment flight and its probability in the polar direction is only 12 to 15 per cent higher [25]. Therefore, it could be more realistic to consider the existence of two types of long range particle emission which differ by some properties.

In our experiment the LR-particles were registered by a detector arranged along the fragment flight. The mean angle of particle registrations with respect to the fragment flight taking into account the set-up geometry and the LR-particle angular distribution was about 14°. Rather small statistics were obtained in the measurements (3650 and 760 events corresponding to the LR-particle flight toward the light and heavy fragment, respectively). Therefore, a successive file of stored events could be used in data processing what in turn made it possible to use the information on the LR-particle energy. At the same time, due to small statistics it was not possible to perform any unfolding of the neutron multiplicity distributions and toobtain any information for fixed combinations of neutron numbers.

The mean values ofsome quantities of this process are presented in Table 9. It can be seen that if in the case of equatorial emission the fragments are less deformed or excited than in binary fission, in the case of polar emission the fragment deformation or excitation are close to those in binary fission. At the same time, the fragment total kinetic energy is in this case rather less than in binary fission or in ternary fission with equatorial emission.

A pronounced asymmetry can be noted in the numbers of neutrons emitted by the light and heavy fragments. It is seen both from Table 8 and Fig. 29 where the mean neutron emissions

Table 8

Mean values of various quantities in ternary fission of ^{252}Cf with polar emission of LR-alphas.

	Flight toward light fragment	Flight toward heavy fragment
M_L, a.m.u.	108±1	110±1
M_H, a.m.u.	140±1	138±1
E_k, MeV	168.0±0.5	170.0±1.0
ν_T	3.54±0.09	3.54±0.15
ν_L/ν_H	2.16	1.44
Statistics	3625	748

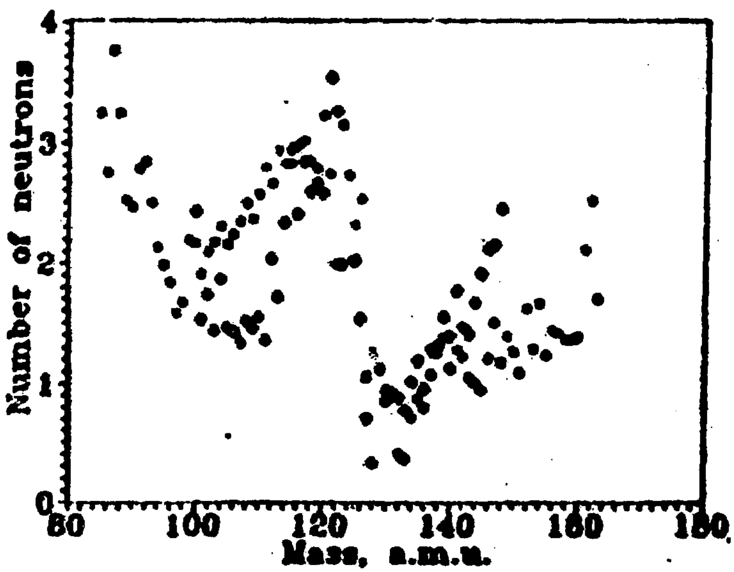

Fig. 29. The mean neutron emission in ternary fission with polar emission of LR-particles as a function of fragment mass:

● - LR-particle flight toward the light fragment;

⊕ - LR-particle flight toward the heavy fragment.

from individual fragment are presented as a function of fragment masses for the cases of LR-particle flights toward the light and heavy fragments. The curves presented have a conventional saw-tooth shape, though in the first case there is a rise of ν in the region of lightest masses ($85 < M_L < 95$). In the second case, there is no statistics available in this mass region. In this case, the asymmetry is somewhat less and heavy fragments themselves are more deformed or excited than in the previous case. However, the light fragments are still more deformed than the heavy ones.

The information obtained suggests a conclusion that the polar emission towards the light fragment occurs mainly in the case of strongly deformed light fragments with rather compact configuration of their heavy complements. In the case of emission towards the heavy fragments the difference between the neutron numbers or fragment deformations are noticeable less and the heavy fragments are more deformed than in the previous case. Nevertheless, in this case the light fragments are still more deformed than the heavy ones ($\nu_L/\nu_H = 1.44$).

The fragment mass distributions for both the cases are presented in Fig. 30. As it was mentioned earlier, a pronouced yield of the mass $M = 132$ should be expected in the case of strongly deformed light fragments. However, no proper peaks are seen in the distributions and the yields of this mass amounts to a half of the maximal ones. In the similar mass distribution obtained in [25] this mass is somewhat more pronounced and manifests itself as a bend of the curve.

The mass distribution concidered for the case of LR-particle flight towards the light fragment looks like that in ternary fission with equatorial emission for the case of an intermediate deformation of the light fragment and a compact deformation of the heavy fragment, when the yield of the mass $M_H = 132$ is still isufficiently pronounced, the masses $M_L = 112$ and $M_H = 140$ prevail in binary fission and the main mass shift due to the LR-particle emission falls on the light peak. In this case in ternary fission with equatorial emission the mean

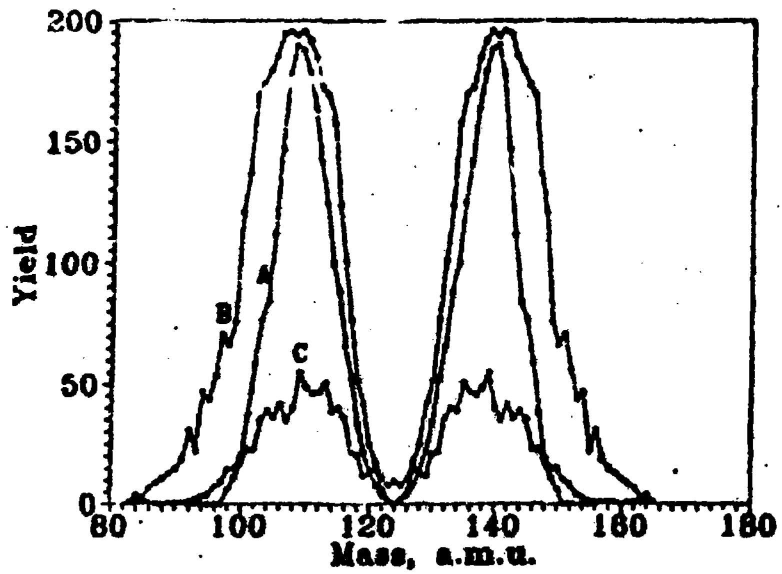

Fig. 30. The mass distributions in ternary fission with polar emission toward the light (A) and heavy fragments (C) in comparison with that in ternary fission with equatorial emission for the (2|1) combination of fixed neutron numbers

masses M_L = 108, M_H = 140. are the same as in the distribution concidered. A comparison of this distribution with that for the case of equatirial emission for the combination of neutron numbers (2|1) is presented in Fig. 30.

The mean masses obtained in [25] are M_L = 109, M_H = 139. The mean masses obtained in our measurements in the case of emission towards the heavy fragments are shifted by 2 a.m.u. with respect to those in the other case and are M_L = 110, M_H = 138. The mean masses from [25] are the same for both the cases and the mass distributions themselves are rather similar. It should be noted that poor statistics for the second case either in our measurements or in [25] makes determination of the mean masses uncertain.

In conclusion, the mass distribution in ternary fission with polar emission can be assumed to be governed mainly by the minimum C and in part by the minimum C on the plot by WILKINS and the emission of LR-particles occurring from a single fragment.

Fig. 31 presents the mean neutron emission as a function of LR-alpha energy. These curves have nonlinear character and show a sudden change in the slope at E_α = 18 MeV. Besides, they have a concave shape instead of the prominent shape obtained in [22] for a similar dependence in equatorial emission. The derivative $d\nu_T/dE_\alpha$ does not depend on the fragment mass as well as in [22] for the case of equatorial emission.

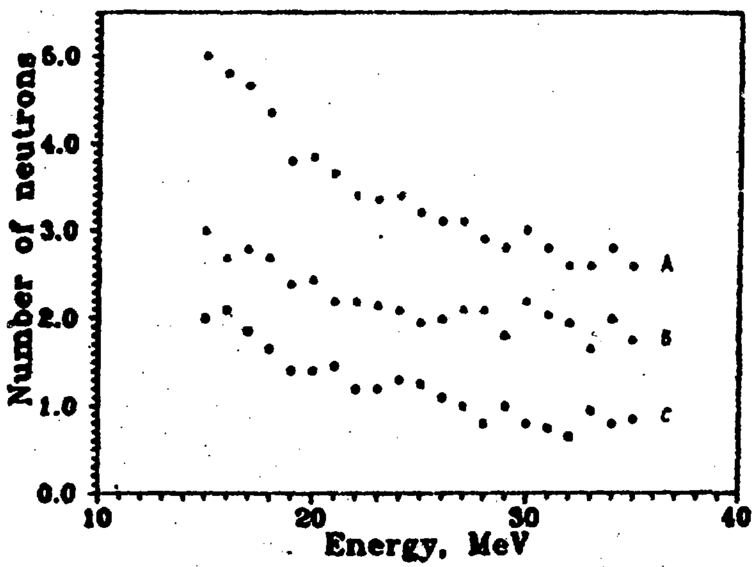

Fig. 31. The mean total neutron emission (A) and the mean emission from individual light (B) and heavy (C) fragment in ternary fission with polar emission as a function of the LR-particle kinetic energy

Fig. 32 presents the fragment total kinetic energy as a function of the LR-alpha energy. This curve is nonlinear in shape as before and has a sudden break at the same 18 MeV-energy. Its slope dE_k/dE_α now depends on the fragment mass (Fig. 33) as well as a similar derivative from [22] for the case of equatorial emission. However, the character of this dependence is reverse of that obtained in [22]. If in the case of equatorial emission the slope rises when approaching the symmetric mass split, then by contrast in the case of polar emission it falls down, and within an appreciable mass range (110 to 124) the fragment total kinetic energy does not depend on the LR-alpha kinetic energy. This could probably result from a different character of the acceleration of LR-particles emitted from the neck region or from the outside part of the fragment surface.

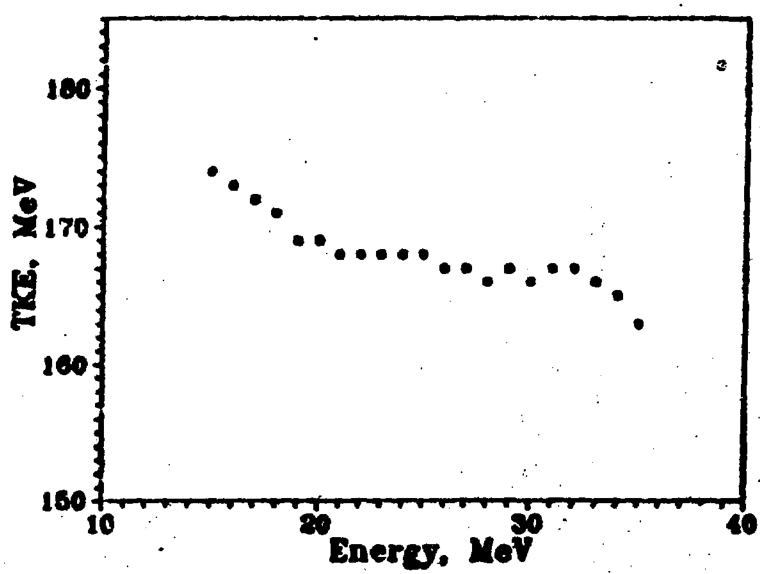

Fig. 32. The total fragment kinetic energy in ternary fission with polar emission as a function of the LR-particle kinetic energy

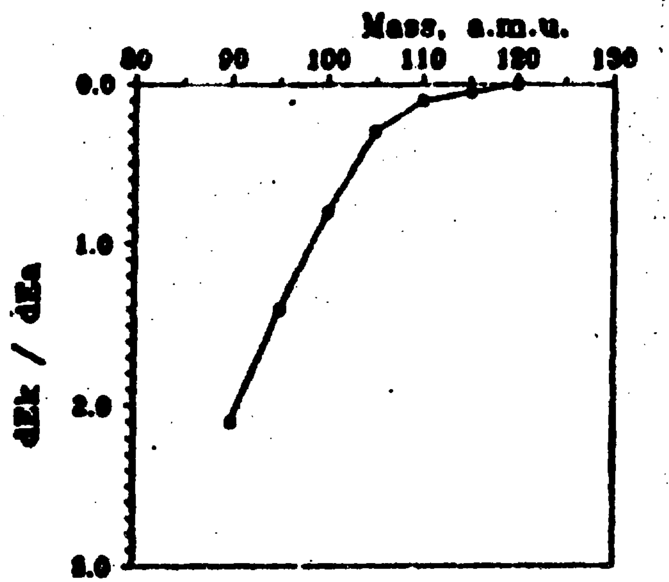

Fig. 33. The slope $dTKE/dE_{\alpha}$ as a function of fragment mass

CONCLUSION

Analysis of the partial mass distributions corresponding to fixed numbers of prompt neutrons makes it possible to trace the dependence of the mass distribution formation on thefragment deformation and make some conclusions on the character of the potential energy surface in the scission point. The picture obtained agrees mainly with that obtained by WILKINS (3), but suggests a possible presence of an extended valley responsible for a significant part of the mass distributions. Visible correlations of behaviour of both the fragments show that statistical calculations using a one-dimensional energy surface which characterizes a formation of single fragments can give only a rough description of the mass distribution formation. To provide a more adequate picture, a multi-dimensional energy surface should be used to account for simultaneously thedeformations of both the fragments, the mass division, the charge distributions and so on, for example, as obtained in [26].

If one considers the information obtained from the viewpoint of the model proposed by BROSA and GROSSMAN [4,5], then the 107/145 mass split can be regarded as an initial scission configuration, though featuring various degrees of deformation (cf. cases (0|0) to (3|3)) and the uniform drift of mass distribution peaks from this starting point towards either asymmetric or symmetric mass splits with the fragment deformation variations as well as deformation partitions between the fragments definitely connected with this drift could be assumed to be governed by a position of the neck rupture point. Besides, superlong configurations predicted by BROSA and GROSSMAN are really observed both in the extremely asymmetric mass split and in symmetric or near symmetric ones ($\nu_T = 5,6,7$).

The structures observed in the distributions obtained suggest that spontaneous fission is a weakly dissipative process and that free energy can be realized as prescission kinetic energy which should be accounted for in the estimation of dynamic effects at the descent from saddle to scission.

Consideration of mass distributions in ternary fission shows that the main contribution in the LR-alpha formation is provided by only one fragment either in equatorial or in polar emission. The α-particle emission occurs at the last stage of the descent to the scission point when the mass distribution is already formed, and the scission configurations in binary and ternary fission are nearly the same. More detailed parameters of the mass distribution formation are very promising. In particular, it is very important to obtain for fixed combinations of neutron numbers the total distributions of fragment mass and kinetic energy. However, it requires statistics to be increased at least by an order or more. An increase in the number of fixed parameters and, in particular, registration of the fragment charges is especially promising. It will make it possible to obtain the picture of shell structures in more detail.

References

1. P.Fong. Statistical Theory of Nuclear Fission. Gordon and Breach (1969).
2. J.A.Maruhn et al. Heavy Ion Collisions. North-Holland, Amsterdam, 11, 397 (1980).
3. B.D.Wilkins et al. Phys. Rev. C14, 1832 (1976).
4. U.Brosa et al. Z. Phys, A310, 177 (1983).
5. U.Brosa et al. Z. Naturf., 41a, 1341 (1986).
6. C.Signarbieux et al. In Proc. of Internat. Conf. on Physics and Chemistry of Fission (Rochester), 2, 179 (1973).
7. A.Gavron, Z.Fraenkel. Phys. Rev. Lett., 27, 1148 (1971).
8. H.Nifenecker et al. Ref. 6, p. 117.
9. G.Bareau et al. In Proc. of Internat. Conf. on Nucl. Data for Basic and Appl. Sci. Santa Fe, USA, 1985, p. 409.
10. J.P.Theobald. In Proc. of Internat. Conf. on Nucl. Data for Sci. and Technology, Antwerp, Belgium, 1982, p. 719.
11. R.L.Walsh. Ref. 6, p. 357.
12. G.Mariolopoulos et al. Nucl. Phys. A361, 213 (1981).
13. A.C.Wahl. Atomic Data and Nuclear Data Tables, 39, 1 (1988).
14. R.W.Hasse. Preprint GSI, Darmstadt, FRG, 1987, GSI-87-24.
15. P.Koczon, thesis, Darmstadt, 1987.
16. A.A.Aleksandrov et al. Report presented to the Internat. Conf. "50-th Aniversary of Nucl. Fission", Leningrad, 1989.
17. J.R.Nix, W.J.Swiatecki. Nucl. Phys., 71, 1 (1965).

18. I.A.Mitropolski, A.G.Shuvaev. Preprint n'1075 of Leningrad Institute of Nucl. Physics, Leningrad, 1985.
19. I.D.Alkhazov et al. Sov. Nucl. Phys. 48, 1635 (1988).
20. G.Garvey et al. Rev. Mod. Phys., 41, S1 (1969).
21. E.Nardi, Z.Fraenkel. Phys. Rev. C, 2, 1156 (1970).
22. G.K.Mehta et al. Phys. Rev. C, 7, 373 (1971).
23. N.Feather. Proc. Royal Soc. Edinburgh, 66A, 192 (1964).
24. I.D.Alkhazov et al. Sov. Nucl. Phys. 48, 655 (1988).
25. M.Mutterer et al. Report presented to the Internat. Conf. "50-th Aniversary of Nucl. Fission", Leningrad, 1989.
26. J.Moreau et al. In Proc. of the "Seminar of Fission", Habay-la-Neuve, Belgium, 1986, p. 101.

Редактор Н. П. Деева

Подписано в печать 28.03.91. Формат 60 x 90 1/16
Офсет. печ. Печ. л. 3. Уч.-изд. л. 2,1. Тираж 130 экз.
Заказ № 139 Цена 42 коп. Индекс 3624

Отпечатано в НПО "Радиевый институт им. В. Г. Хлопина"
194021, Ленинград, пр. Шверника, 28

42 коп.

Индекс 3626

Препринт РМ-225. М., 1991, 1 - 47